Fuel 120 (2014) 218–232

Contents lists available at ScienceDirect

Fuel

journal homepage: www.elsevier.com/locate/fuel

Determination of mass transfer parameters in solvent-based oil recovery techniques using a non-equilibrium boundary condition at the interface

S. Reza Etminan *, Brij B. Maini, Zhangxin Chen

Chemical & Petroleum Engineering Department, University of Calgary, Canada

HIGHLIGHTS

- Dilute dissolution of gases into heavy oil was modeled accounting for 3 parameters.
- The unknown parameters were diffusion and mass transfer coefficients, and solubility.
- 3 Mass transfer parameters were measured through running one diffusion experiment.
- Sensitivity coefficients were applied to find the sensitivity of *P* to each unknown.
- Closer to onset of asphaltene precipitation, the interface resistance becomes larger.

ARTICLE INFO

Article history:
Received 29 August 2013
Received in revised form 11 November 2013
Accepted 12 November 2013
Available online 2 December 2013

Keywords:
Molecular diffusion coefficient
Mathematical modeling
Parameter identification
Interface
Resistance

ABSTRACT

Having a reliable estimate of gaseous-solvents molecular diffusion coefficients in heavy oil and bitumen is a requisite for analysis and design of gas injection and solvent-based recovery techniques. Nevertheless, diffusion coefficient is not measured accurately unless all other contributing mass transfer parameters are considered, included in the modeling, and estimated correctly. These other parameters are gas solubility and interface resistance, of which the latter is represented by mass transfer coefficient term. In this work, an analytical model is introduced in conjunction with an inverse technique to obtain these three abovementioned parameters using a single pressure decay data set. Sensitivity coefficient analysis is applied as an additional practical evaluation tool to display the sensitivity of the measured pressure to each of the unknown parameters. Characterization of the interface resistance as a physical phenomenon which hinders the molecular diffusion of gas through the interface and complicates the modeling is further investigated in this work. Incipient asphaltene precipitation in heptane–toluene–asphaltene mixture was chosen as a potential phenomenon which alters the interfacial resistance. It is shown that our proposed inverse analysis locates the unknown parameters correctly when history matching per se is not disclosing all the sufficient information for accurate parameter estimation.

1. Introduction

In many oil sand reservoirs, bitumen viscosity is so high that it is not mobile at the reservoir condition. For this oil to be producible, viscosity must be reduced either by heat or by dilution. Using solvents not only reduces the viscosity by dilution, but it can also cause de-asphalting. This latter phenomenon upgrades the bitumen and leaves the heavier components inside the reservoir. In these processes, mass transfer parameters become important because they control the rate of dilution. Diffusion coefficient and solubility are two basic mass transfer parameters in dissolution of solvent gases into heavy oils. The first coefficient shows the rate of dissolution and the second one expresses the ultimate amount of gas dissolution into heavy oil. Therefore, knowledge of these two parameters is necessary for designing solvent-based production schemes in these reservoirs. They could also be utilized in compositional reservoir simulators to forecast the recovery.

Among momentum, heat and mass transport processes, heat conduction and viscosity have standardized techniques for measurements. However, it is not the same for the diffusion coefficient; and measurements of mass transfer characteristics are often more challenging, specifically due to difficulties in measuring point values of concentration and other issues like: phase equilibrium, effect of convective transport and having a mixture rather than a pure fluid [1]. There are a few experimental methods to estimate the magnitude of gas diffusivity in a liquid. In one category of these techniques, the measurement is based on determination of the concentration of the diffusing gas along the diffusion path in the liquid with time. This technique needs compositional analysis and its downsides are numerous. They are system-intrusive, very

* Corresponding author. Tel.: +1 (403) 210 5363.
E-mail address: sretmina@ucalgary.ca (S.R. Etminan).

0016-2361/$ - see front matter © 2013 Elsevier Ltd. All rights reserved.
http://dx.doi.org/10.1016/j.fuel.2013.11.027

Nomenclature

A	diffusion cell cross sectional area, m^2
C	mass concentration, kg/m^3
D	diffusion coefficient, m^2/s
E	Objective function
H	Henry's law constant, $MPa/(kg/m^3)$
h	height of bitumen column, m
J	sensitivity matrix
k	film mass transfer coefficient, m/s
L	vector of unknown values
M	group of coefficients
Mw	molecular weight, $kg/(kg-mole)$
m	mass of gas dissolved, kg
N	group of coefficients
P	pressure, MPa
R	universal gas constant, 0.0083144 $MPa\ m^3/kg-mol\ K$
T	absolute temperature, K
t	time, s
V	volume, m^3
w	gas mass fraction
Z	gas compressibility factor
z	vertical spatial coordinate, m

Greek letters

ρ	density of mixture, kg/m^3
λ	eigen-value
ρ	damping parameter
Ω	diagonal matrix

Superscripts

Asterisk	chemical equilibrium condition
n	time step coefficient
q	iteration number
T	transpose

Subscripts

b	bitumen
$comp$	computed
exp	experimental
eq	equilibrium
g	gas
gc	gas cap
i	initial condition
int	interface
m	mass
p	eigen values index
r	relative

Abbreviations

BC	Boundary Condition
C7	heptane, C_7H_{16}
MM	Million
LM	Levenberg Marquardt
SAGD	Solvent Assisted Gravity Drainage
CSS	Cyclic Steam Stimulation
VAPEX	Vapour Extraction
EOS	Equation Of State
rms	root mean square

expensive, time consuming and labor intensive [2–4]. There are other methods that measure a dissolution-dependent property like pressure, solvent volume, or cumulative mass of dissolution and use this property to calculate diffusivity. These methods are referred to as indirect methods and have been referenced in many publications [1,5–11].

Within all these methods, the Pressure Decay technique introduced by Riazi [8] and Sachs [9] is a simple and highly reliable method. In this method, a high pressure constant volume diffusion cell is used in an isothermal condition. Heavy oil sample is placed at the bottom of the high pressure cell as a quiescent liquid column. At this time, the gas cap is pressurized to a certain pressure and then disconnected from the gas supply. Having constant gas-oil compositions in the cell, gas cap pressure starts to drop as a result of diffusion of the gas molecules into the heavy oil. This pressure drop is recorded with time and is used later in mathematical diffusion models to estimate mass transfer parameters. This technique has been applied by many authors to characterize mass transfer of gases into heavy oil and bitumen [5,8–10,12–21].

Different mathematical models have been introduced for modeling diffusion experiments and locating the unknown parameters using the pressure decay method. These models and their solutions are dissimilar in terms of the interface thermodynamic conditions, simplifying assumptions and parameter estimation algorithms. In addition to the diffusion coefficient and solubility, gas-oil interfacial resistance is another coefficient to be considered in the modeling and parameter estimation of the diffusion processes. There are many works published on determination of the first two assuming that no interfacial resistance exists [1,5,7,8,10,15,16,19]. However, only limited models [12–14,21–24] exist in the literature which considers the resistance at the interface of gas-oil as well. This interfacial resistance is introduced in our calculations through reciprocal value of film mass transfer coefficient (k).

Tharanivasan et al. [16] studied different transport conditions at the interface based on the work of Zhang et al. [19], Upreti and Mehrotra [10] and Civan and Rasmussen [13] and categorized the boundary conditions used at the interface of these three works as equilibrium, quasi-equilibrium and non-equilibrium, respectively. When no gas concentration discontinuity (in the liquid phase) exists across the interface (right above and below the interface have the same concentration), the equilibrium term is used. Once passage of solvent molecules through the gas–liquid interface is hindered, the non-equilibrium term is applied. In the first case, the interfacial resistance term ($1/k$) goes toward zero as the mass transfer coefficient (k) takes very large value. This allows removal of the resistance term from the whole modeling and simplifies the parameter estimation with one less parameter to be found. Otherwise, interfacial resistance should be included into the modeling and be estimated. Based on the preceding classification, the models of Riazi [8], Zhang et al. [19], Sheikha et al. [5], Etminan et al. [1] would all be categorized as employing equilibrium boundary conditions.

On the other hand, from 2001 to 2009, Civan and Rasmussen model and their proposed inverse technique [12–14,22,23] remain the single diffusion model with non-equilibrium boundary condition in the related literature. They suggested a boundary condition which accounted for a possible hindrance in gas diffusion due to interfacial resistance and solved Fick's second law using their Robin-type boundary condition while keeping saturation concentration constant at the interface. Robin or third-type BC is a linear combination of a prescribed concentration and mass flux on the boundary of the domain. Their analytical solution is simplified to

a short time solution, an asymptotic behavior of the short time solution in very large values of dimensionless time, and a long-time (finite acting) solution. Their inverse method was a graphical method determined through the Separation of Variables technique for solution of diffusion partial differential equations. Using the first eigen-value in large time, they linearized the solution and used the "slope-intercept" technique to find the unknowns. The unknown eigen-value was determined from the intercept and through finding roots of a trigonometric equation. Using the eigen-value, diffusion coefficient was obtainable from the slope. Finally, a transcendental equation needed to be solved to get the value of mass transfer coefficient. The "slope-intercept" technique is applicable in large-time solution and in their other two proposed solutions for short-time; a least-squares curve fitting technique was applied to find the values of the unknown parameters.

Recently, Etminan et al. [21] developed a semi-analytical diffusion model which considers the interfacial resistance through a time-dependent Robin boundary condition. This boundary condition is able to model both equilibrium and non-equilibrium at the interface. Unlike the other available solutions for modeling the interfacial resistance, this model accounts for the relationship between gas cap pressure decline and concentration at the interface. It allows for the change of interface concentration with the decaying pressure and does not apply the late-time saturation concentration in the interface boundary condition (which is not valid for the entire course of the experiment). Through this work, it was shown that the size of the gas cap becomes important in Civan and Rasmussen's [13] solution and use of saturation concentration at the interface is accurate when the gas cap pressure decline due to dissolution, is small and close to the equilibrium pressure in saturation concentration. This latter could lead to underestimation of the rate of gas dissolution and consequently, diffusion coefficient. The detail of the direct model verification and its comparison with the previous models are presented in Etminan et al.'s work [21]. Therefore, for the sake of brevity, they are not repeated here.

In this work, the semi-analytical method of Etminan et al. [21] is applied in combination with a regularization scheme that is a damped least-squares technique, the Levenberg–Marquardt method, to find the mass transfer parameters in Pressure Decay experiments. Several experiments were conducted using the pressure decay technique in different scenarios. The measured pressure data was used along with the computed pressure values from our model to form the objective function. Through this technique, the values of diffusivity, solubility (saturation concentration) and interface resistance are estimated. Determination of these parameters sheds light on answering these questions: (i) How the values of each of these physical mass transfer parameters change and the order of their change; (ii) if there exists resistance at the interface of solvent–bitumen systems; (iii) If the presence of poorly solubilized asphaltene could be a reason for interface resistance? The accuracy of the estimated parameters was examined using available data in the literature and the uniqueness and area of uncertainty of each parameter value was obtained.

2. Theory and mathematical model

2.1. Direct problem

The pressure decay experimental technique involves a constant volume, constant composition system. Solvent gas leaves the gas cap and diffuses into the heavy oil body through their interface. Assuming that heavy oil or bitumen does not have any volatile component to diffuse into the gas, focus is on the unidirectional diffusion of solvent gas into the bitumen body. Therefore, the control volume of our mathematical model is only the liquid column.

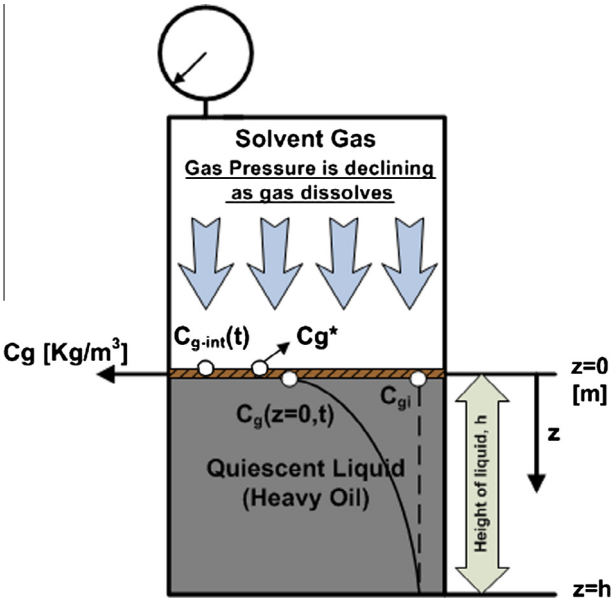

Fig. 1. Schematic of pressure decay cell and interface concentrations in presence of film resistance.

Fig. 1 displays a schematic of a pressure decay cell and an exaggerated interface resistance layer between the heavy oil and gas cap.

For a planar geometry and one dimensional linear diffusion process, Fick's second law describes the gas concentration distribution as a function of spatial position and time as follows:

$$\frac{\partial^2 C_g}{\partial z^2} = \frac{1}{D}\frac{\partial C_g}{\partial t} \tag{1}$$

The associated initial condition is the heavy oil or bitumen to be free of dissolved gas.

$$C_g(z, t = 0) = 0 \tag{2}$$

The spatial coordinate will be set at the interface such that the interface takes the value of $z = 0$ and the cell's bottom is at $z = h$. The diffusion cell's bottom is closed and therefore, our domain is a finite domain. As there is no gas diffusion beyond $z = h$, a no-flow boundary condition is assigned to it as:

$$\left.\frac{\partial C_g}{\partial z}\right|_{z=h} = 0 \tag{3}$$

In order to investigate the effect of resistance at the interface, a time-dependent third-kind boundary condition was introduced and investigated by Etminan et al. [21]. This boundary condition relates the rate of transfer at the interface to the difference between the actual liquid-phase concentration, $C_g(z = 0,t)$, at the interface at any time and the concentration, $C_{g\text{-}int}(t)$, which would be in equilibrium with the pressure in the gas cap:

$$-D\left.\frac{\partial C_g}{\partial z}\right|_{z=0} = k(C_{g\text{-}int}(t) - C_g(z = 0, t)) \tag{4}$$

A schematic of these two concentrations and a sample concentration profile is depicted in Fig. 1. Assuming that the exaggeratedly thick crosshatched region is where the interface resistance shows its effect, $C_g(z = 0,t)$ is referred to as concentration right below the interface and $C_{g\text{-}int}(t)$ as concentration right above the interface. A similar boundary condition involving a mass-transfer coefficient, k, was used earlier by Civan and Rasmussen [12–14]. It is a more general and the non-equilibrium form of Sheikha et al. [5]'s boundary condition. Etminan et al. [21] have shown that in the case of no resistivity when k goes to very large values, these

two boundary conditions and subsequently their two solutions for concentration distributions are identical. Henry's law constant was used for relating the gas cap pressure to the instantaneous equilibrium concentration at the interface, $C_{g\text{-}int}(t)$, as in the following equation:

$$C_{g\text{-}int}(t) = \frac{P(t)}{H} \tag{5}$$

In this boundary condition, the interface concentration $C_{g\text{-}int}(t)$ changes with reducing pressure in the gas cap and is not assumed to be constant. The following simplifying assumptions were applied in solution of our analytical model. Evaluation of some of these assumptions and validity of their use are investigated by Etminan et al. [21].

1. Oil is motionless and its swelling due to gas dissolution is negligible (dilute solutions).
2. Gas diffusion is unidirectional and oil is non-volatile ($n_{bz} = 0$).
3. Solution density change is assumed negligible (it is correct only in dilute solutions).
4. The diffusion coefficient is constant.
5. There is no chemical reaction between the diffusing gaseous solvent and oil.
6. Natural convection does not occur.
7. The gas compressibility factor is assumed to be constant over the pressure range involved in the test.

The Laplace transform technique was applied using the preceding initial and boundary conditions. The solution of Eqs. (1)–(4) in the Laplace domain becomes:

$$\overline{C}_g(z,S) = \frac{MP_i\left[\exp(\sqrt{\frac{S}{D}}(z-2h) + \exp\left(-\sqrt{\frac{S}{D}}z\right)\right]}{H\left[\left(MS + (1+NS)\sqrt{\frac{S}{D}}\right) + \exp\left(-2\sqrt{\frac{S}{D}}h\right)\left(MS - (1+NS)\sqrt{\frac{S}{D}}\right)\right]} \tag{6}$$

In this equation, S denotes the variable of the frequency domain; M and N are defined in Eqs. (7) and (8) and $\overline{C}_g$ is the gas concentration in the Laplace domain.

$$M = \frac{V_{gc} \cdot Mw \cdot H}{AZRTD} \tag{7}$$

$$N = \frac{V_{gc} \cdot Mw \cdot H}{AZRTk} \tag{8}$$

where V_{gc} is the volume of the gas cap, Mw is the gas molecular weight, A is the diffusion cell cross-sectional area, H is Henry's law constant, Z is the gas compressibility factor, R is the universal gas constant and T is the absolute temperature. If Eq. (4) is written using Henry's law constant in order to relate $C_{g\text{-}int}(t)$ to $P(t)$, then Eq. (9) is obtained.

$$P(t) = -\frac{DH}{k}\frac{\partial C_g}{\partial z}\bigg|_{z=0} + HC_g(z=0,t) \tag{9}$$

If the calculated pressure is called P_{comp}, its value in the Laplace space is:

$$\overline{P}_{comp} = -\frac{DH}{k}\frac{\partial \overline{C}_g}{\partial z}\bigg|_{z=0,S} + H\overline{C}_g(z=0,S) \tag{10}$$

Applying the PDE solution, Eq. (6), to Eq. (10) leads to the value of P_{comp} in the Laplace space as:

$$\overline{P}_{comp}(S) = \frac{MP_i\left(\left[\exp\left(-2h\sqrt{\frac{S}{D}}\right)+1\right] - \frac{D}{k}\left[\sqrt{\frac{S}{D}}\exp(-2h\sqrt{\frac{S}{D}}) - \sqrt{\frac{S}{D}}\right]\right)}{\left[\left(MS + (1+NS)\sqrt{\frac{S}{D}}\right) + \exp\left(-2\sqrt{\frac{S}{D}}h\right)\left(MS - (1+NS)\sqrt{\frac{S}{D}}\right)\right]} \tag{11}$$

where $\overline{P}_{comp}$ is the predicted gas cap pressure in the Laplace domain. An analytical closed-form of the Laplace inverse of Eq. (10) is not available; therefore, the Stehfest algorithm was applied to find the inverse form numerically [25]. This solution allows us to produce pressure values with respect to time which can be easily used in combination with the pressure decay raw data to estimate the unknown parameters.

2.2. Inverse problem and numerical optimization

Diffusion of gas into the liquids is a "cause-effect" relationship. Based on the mathematical model explained in the previous section, the *causal* characteristics of gas mass transfer in the oil body are boundary conditions and their parameters, initial conditions, diffusion coefficients of gas and liquids into each other, interface resistance and ultimate solubility as well as geometric characteristics of the body or the system. Then the *effect* is a state which is determined by the concentration distribution field. The purpose of the direct problem is to specify the cause-effect relationship. On the other hand, if it is required to recover causal characteristics and parameters from definite information about the concentration field, we have a statement of an inverse problem. The statement of inverse problems, unlike the direct ones, cannot be reproduced in actual experiments; i.e., it is not possible to reverse the cause-effect relationship physically instead of mathematically [26]. Based on Alifanov [26], in mathematical formalization, the characteristics of this problem manifests itself as "incorrect" mathematical conditioning and inverse problems present a typical example of ill-posed problems. For the class of ill-posed problems, the solution should necessarily exist, be unique and also be stable [27].

Generally, inverse problems are solved by minimizing an objective function with some stabilization techniques used in the estimation procedure [28]. In this problem, the objective function, E, which provides minimum variance estimates, is the ordinary least squares norm (or sum of squared residuals).

$$E(L) = \sum_{i=1}^{n}(P_{\exp}(t) - P_{comp}(t))^2 \tag{12}$$

In this equation, $P_{\exp}$ is the experimental measured pressure values vector, P_{comp} is the computed pressure based on our semi-analytical model, n is the number of measured pressure values and L is the vector of unknown mass transfer parameters, to be estimated through the inverse solution.

$$\vec{L} = [L_1, L_2, L_3]^T = [k, H, D]^T \tag{13}$$

$$E(\vec{L}) = (\vec{P}_{\exp} - \vec{P}_{comp})^T(\vec{P}_{\exp} - \vec{P}_{comp}) \tag{14}$$

Eq. (14) is the vector form of Eq. (12) in which $\vec{P}^T_{\exp} = [P_{\exp 1}, P_{\exp 2}, \ldots, P_{\exp n}]$ is the vector of measured pressure obtained by experiments at n points, $\vec{P}^T_{comp} = [P_{comp1}(\vec{L}), P_{comp2}(\vec{L}), \ldots, P_{compn}(\vec{L})]$ is the vector of computed pressure at each time obtained from the solution of the direct problem with an initial estimate for vector L components and T is the transpose sign.

Based on Ozisik and Orlande [28], to minimize the least squares norm given by Eq. (12), the derivatives of $E(\vec{L})$ need to be zero with respect to each of the unknown parameters k, H and D.

$$\frac{\partial E(\vec{L})}{\partial L_1} = \frac{\partial E(\vec{L})}{\partial L_2} = \frac{\partial E(\vec{L})}{\partial L_3} = 0 \tag{15}$$

The matrix notation of this necessary condition for the minimization of $E(\vec{L})$ can be represented by gradient of $E(\vec{L})$ which should be zero with respect to the components of vector L.

$$\nabla E(\vec{L}) = 2\left[-\frac{\partial \vec{P}^{T}_{comp}(\vec{L})}{\partial \vec{L}}\right][\vec{P}_{\exp} - \vec{P}_{comp}(\vec{L})] = 0 \quad (16)$$

where

$$J(\vec{L}) = \left[-\frac{\partial \vec{P}^{T}_{comp}\left(\vec{L}\right)}{\partial \vec{L}}\right]^{T} \quad (17)$$

is the *sensitivity* or *Jacobian* matrix. This matrix plays a very important role in parameter estimation problems (Appendix A). Three mass transfer parameters are determined through minimization of $E(\vec{L})$ with respect to each of them. This is accomplished by using a modified form of the Gauss–Newton method [28,29] for the solution of non-linear least square problems. This modification involves adding a regularization parameter to reduce instabilities [28]. This method is called the Levenberg–Marquardt (LM) method [27,28,30] which is given by the following iterative form:

$$\vec{L}^{(q+1)} = \vec{L}^{(q)} + [(J^{(q)})^{T}J^{(q)} + \mu^{(q)}\Omega^{(q)}]^{-1} \times (J^{(q)})^{T}[\vec{P}_{\exp} - \vec{P}_{comp}(\vec{L}^{(q)})] \quad (18)$$

in which the superscript q is the iteration number and J is the sensitivity matrix calculated at the iteration q. In this equation, $\mu^{(q)}$ is a positive scalar named damping parameter and $\Omega^{(q)}$ is a diagonal matrix defined as:

$$\Omega^{(q)} = diag[(J^{(q)})^{T}J^{(q)}] \quad (19)$$

The matrix term $\mu^{(q)}\Omega^{(q)}$ is used to damp the oscillations and instabilities due to ill-conditioned character of such problems. In practice, the Levenberg–Marquardt method is combination of the Steepest Descent and Gauss–Newton methods. At the beginning of iterations, in which the initial guess can be far from the exact parameters, the damping factor becomes large and this cancels off the role of matrix $(J^{(q)})^{T}J^{(q)}$ which is almost singular in this region. Therefore, very small steps are taken in the negative gradient direction and the LM method tends to the Steepest Descent method. Once the iteration procedure approaches the solution of the parameter estimation, the parameter $\mu^{(q)}$ is gradually reduced and the LM method tends to the Gauss–Newton method. The initial value of μ used in this study was 0.0001. The stopping criterion that was used to terminate the iteration procedure was as follows:

$$\|\vec{L}^{(q+1)} - \vec{L}^{(q)}\| = \left((\vec{L}^{(q+1)} - \vec{L}^{(q)})^{T} \times (\vec{L}^{(q+1)} - \vec{L}^{(q)})\right)^{1/2} < \varepsilon \quad (20)$$

where $\|\cdot\|$ is the Euclidean norm defined as above and ε is an arbitrary small number which in our case was 0.0001.

The inversion results were produced using our own Levenberg–Marquardt code in Matlab® programming platform. The accuracy of our code was examined using the data presented in Mittrapiyanuruk's work [30]. The spatial domain was subdivided into 30 intervals, while the time interval of 60 sec was used to advance the solution from zero to final-time (t_{final}) of stopping the experiment. The final-time value and thickness of the liquid domain are different in different experiments under investigation.

The simulated pressure decay (P_{comp}) is obtained using the direct problem solution and through applying a priori prescribed values for the unknown mass transfer parameters. The idea about these initial values' order of magnitude was determined from simple calculation on our own row data (mostly for solubility), previous works or through a global search method [17] in different intervals. A three-parameter search method was conducted for each of the experiments (i) to give an idea of initial guesses where we had no intuition about their order of magnitudes and (ii) to examine and confirm that our optimized parameters from the Levenberg–Marquardt method were globally correct and unique. This search method is tedious but correct and reliable. The estimated parameters from our proposed inverse technique were all in agreement with the results of the global search method. In this backup study, our objective function was defined as:

$$\Delta P_{ave} = \sqrt{\frac{\sum_{i=1}^{n}|P_{\exp}(t) - P_{comp}(t)|^{2}_{t=ti}}{n}} \quad (21)$$

Surface plots of global minimums are presented in this work for methane–bitumen experiment. The three parameters search was reduced to two parameters in most of the cases, as we had a solid initial guess about the ultimate amount of dissolution (which is related to H).

3. Experimental study and measurements

The purpose of the experiments presented in this section, is to demonstrate how our proposed mathematical model and parameter estimation technique can be applied to determine the values of unknown mass transfer parameters. The experimental conditions and materials are selected such that they show: how each of these parameters changes, how our mathematical model covers both equilibrium and non-equilibrium interface conditions and distinguishes for the cases with interface resistance and finally, how incipient asphaltene precipitation could produce interfacial resistance to diffusion.

3.1. Pressure decay experimental setup

Our pressure decay experimental setup is an arrangement of a high precision pressure transducer and a high pressure windowed cell maintained at constant temperature. A column of oil was placed at the bottom of the diffusion cell and then gas filled the gas cap portion to a certain pressure. The gas cap was pressurized to our desired initial pressure quickly such that the gas dissolved during pressurization can be neglected. The time for initial pressurization varied from 15 to 30 s. As the gas diffuses and dissolves into the heavy oil body, the gas cap pressure declines. This decay trend was continuously recorded versus time, which acted as the main experimental measurements. A schematic of our experimental setup is depicted in Fig. 2. Visual high pressure diffusion cell was utilized along with a high precision cathetometer (±0.01 of mm) allowing us to track the interface and the oil volume change. This assists us to verify if our "no volume-change" mathematical assumption remains valid during experiments; if not, whether the errors of neglecting it are measureable. The diffusion cell for experiments of part 1 of Section 3.3 had cross-sectional area of 31.67 ± 0.05 cm^2 with the total height of 5.17 ± 0.01 cm. The other diffusion cell used in experiments of part 2 of Section 3.3 had the cross sectional area of 21.40 ± 0.1 cm^2 and total height of 9.47 ± 0.01 cm. The pressure transducer was a 0.0001% resolution ParaScientific® Digiquartz 31K-101. It could measure absolute pressure up to 1000psi (6893 kPa) with a accuracy of ±0.001 psi. The temperature was controlled through our heating/cooling system and can keep the temperature constant within ±0.1 °C of the set value. The whole system was pressurized with helium to around 1000 psi first and all leaks were detected using a digital helium leak test meter and eliminated.

3.2. Materials

For the first two experiments, bitumen and pure gaseous solvents were used. In these two experiments, methane and carbon dioxide were exposed to MacKay bitumen in 30 °C and 23.9 °C, respectively. The density and viscosity of the bitumen were

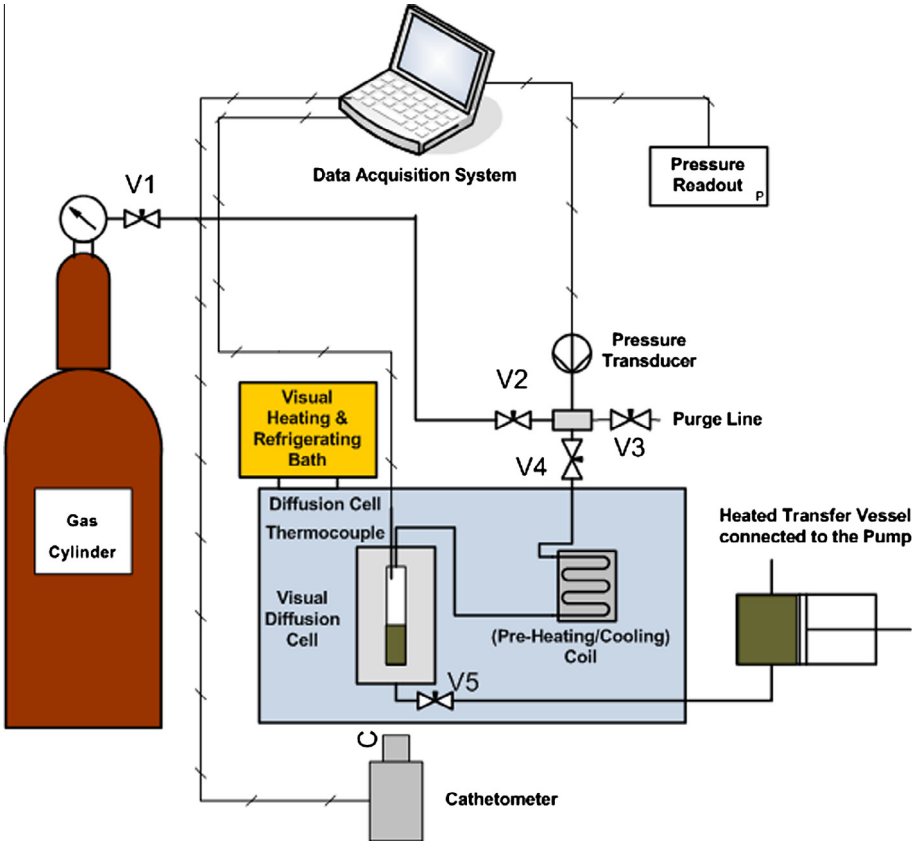

Fig. 2. Pressure decay experimental setup used to measure unknown mass transfer parameters.

Table 1
Properties of conducted experiments using bitumen.

Exp. No.	Diffused gas	Gas purity (%)	Fluid	Pini (Mpa)	Pini (psia)	Height (cm)	Time (days)
1	CO_2	99.9	Pure bitumen	3.5299	512.116	1.605	54
2	CH_4	99.0	Pure bitumen	5.5459	804.59	1.598	82

measured and were respectively 999.368 kg/m^3 and 82,160 mPa s at 30 °C and 1002.689 kg/m^3 and 127,868 mPa s at 23.9 °C. The characteristics of the conducted experiments using CH_4 and CO_2 are listed in Table 1.

In the second set of experiments, heptane (C_7H_{16}), toluene (C_7H_8) and extracted asphaltene particles (from Athabasca bitumen) were used to prepare our liquid sample in different concentrations and pure methane was utilized as the diffusing gas. The purity percentage, molecular weight and density of heptane (C7) and toluene are respectively 99%, 100.21 kg/kg-mole, 684 kg/m^3 and >95%, 92.14 kg/kg-mole, 867 kg/m^3. All experiments in this section were conducted at 20 °C. Table 2 shows the properties of the seven experiments. As it is evident, the samples start from 30 vol.% C7–70 vol.% toluene and its volume concentration goes up to 45 vol.% C7–55 vol.% toluene.

3.3. Experimental scenarios

There are nine experiments presented in this section.

3.3.1. Part 1

The purpose of conducting first two experiments was to display how our mathematical model and parameter estimation technique can estimate the diffusion coefficients, Henry's constant (therefore solubility) and interfacial resistance. In this section, it is also shown how use of sensitivity coefficients interprets our results and allows

Table 2
Properties of heptane–toluene–asphaltene experiments in different concentrations adjacent to the onset of asphaltene precipitation.

Exp. No.	Fluid	C7 (vol.%)	Tol (vol.%)	Asphalt (wt.%)	Density g/cc at 20 °C	Pini (MPa)	Height (mm)
3	Heptane + toluene	30	70	0.63	0.8126	5.519	17.87
4	Heptane + toluene	32.5	67.5	0.61	0.8078	5.522	17.57
5	Heptane + toluene	35	65	0.64	0.8032	5.557	17.92
6	Heptane + toluene	37.5	62.5	0.67	0.7991	5.550	17.81
7	Heptane + toluene	40	60	0.64	0.7941	5.558	18.15
8	Heptane + toluene	42.5	57.5	0.58	0.7905	5.546	18.72
9	Heptane + toluene	45	55	0.58	0.7849	5.520	18.61

to distinguish between equilibrium and non-equilibrium boundary conditions. The results of our estimated parameters are compared with the data available in the literature.

In these experiments, the heated bitumen was pumped from the bottom to our diffusion cell. Then the gas cap was vacuumed while the temperature-controlled water baths kept the temperature at the desired test temperature. As it is seen in Table 1, both experiments were running for extended periods. Reaching pressures closer to equilibrium and having access to the late-time data were the reasons for running these two experiments for this long time. The system was watched continuously for detecting any possible leakage using electronic leak test meters.

3.3.2. Part 2

In the second set of experiments, adsorption of asphaltene molecules at the gas oil interface was evaluated as a possible cause of interface resistance. Adsorption of large molecules at the interface can cause interfacial resistance against gas diffusion. This resistance generates two different concentrations above and below the interface as discussed and causes hindrance in gas diffusion. It is well known that adsorption of surface active molecules can cause interfacial resistance to mass transfer [31–33]. Asphaltene molecules are very polar and exhibit surface active properties. We aimed to investigate how the interfacial resistance ($1/k$) and also other mass transfer parameters change under conditions where asphaltene adsorption at the oil–gas interface is likely to happen. This work does not aim to provide a model for the asphaltene precipitation.

The magnitude of interfacial resistance to mass transfer would be expected to depend on the interfacial concentration of adsorbed molecules [34]. It is also expected that the extent of adsorption would be different in asphaltene solutions prepared in different solvents and that poorer solvents will lead to greater adsorption. The solvent quality was varied by changing the ratio of toluene and heptane in the mixed solvent.

Once gaseous solvent diffuses into heavy oil/bitumen, it dilutes the oil and at the same time, depending on the operating conditions, de-asphalting may occur. Asphaltene exists in the oil as a uniform phase until approaching its instability region. This instability is dependent not only on the properties of asphaltene, but also on how good the rest of the heavy oil/bitumen is a solvent for asphaltene. Therefore, once thermodynamic properties of heavy oil/bitumen change, asphaltene may precipitate and leave the oil phase [35]. Close to the onset of precipitation, polar molecules of asphaltene tend to leave the heavy oil/bitumen and become adsorbed in greater numbers at the available interfaces [36,37].

A common definition for asphaltene is that they are crude oil components that are insoluble in n-alkane (usually n-heptane and n-pentane) and re-dissolvable in aromatic solvents like toluene. Heptane, toluene and asphaltene solid particles (extracted from Athabasca bitumen) were utilized in the experiments of this section to reveal how mass transfer parameters change close to the onset of de-asphalting and see if increased resistance is detected near the incipient precipitation condition. Fig. 3 depicts the experimental results of Alboudwarej et al.'s [38] work. They showed that in a system of heptane–toluene and bitumen, asphaltene is extracted off the bitumen only when the heptane volume fraction is above 40%. It means that below this proportion, the asphaltene molecules experience instability due to micellization mechanism but yet precipitation does not happen. Applying this idea and targeting this region as the most probable condition at which we should expect interface resistance, seven experiments were designed.

The amount of asphaltene solids added to each sample is less than 1 wt.%. A DMA 5000 Anton Paar densitometer was used to measure the density of our samples in each experiment. Fig. 4

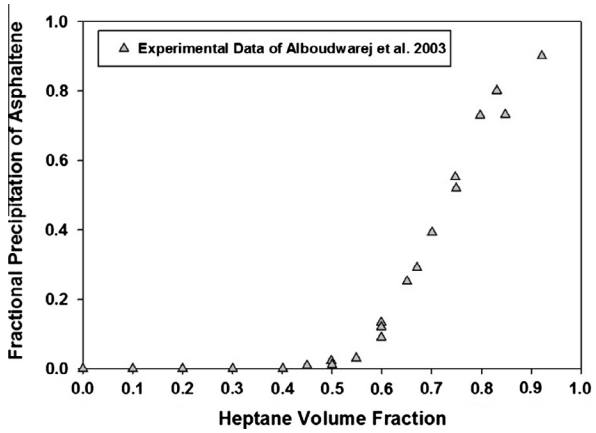

Fig. 3. Fractional precipitation of asphaltene from solution of n-heptane and toluene [38].

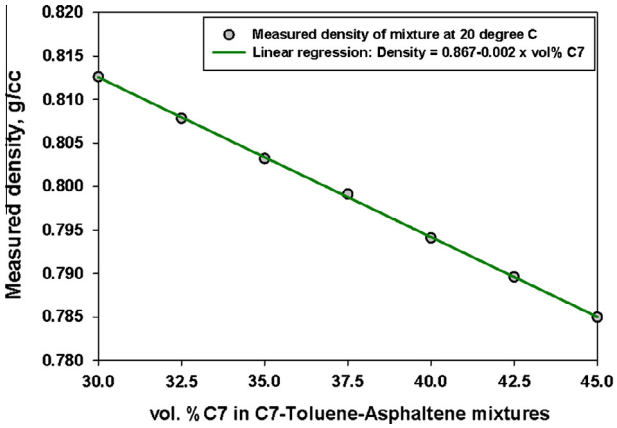

Fig. 4. Change of density of heptane–toluene–asphaltene mixtures with concentration change.

depicts the change of density of the mixture in different concentrations which shows a linear behavior.

For preparation of each sample, the mixture of heptane–toluene was prepared first and then the asphaltene was added into it. All samples were kept in parafilm-sealed jars for at least 24 h after preparations. This time allows the asphaltene to be dissolved to its maximum amount. Figs. 5a and 5b shows the asphaltene particles and the samples before and after adding the asphaltene, respectively. In order to check whether the onset of our samples' asphaltene precipitations are identical with Alboudwarej et al.'s [38] results, the precipitation was checked visually. One and half day after the preparation of each sample, we put the jars to their sides and watched for any sign of precipitated asphaltene. This study agreed with the results of Alboudwarej et al. [38] as change of color in jars only happened in cases of 42.5% and 45%. In the other jars, no precipitation was observed. Figs. 5c and 5d display how clear the bottom of glass jars is for the cases of 35% and 37.5%. Fig. 5e shows how the color of the jar looks brown and a few precipitated particles can be detected. In Fig. 5f, the precipitated asphaltene is easily seen.

4. Data interpretations and parameter estimation

4.1. CO_2 in bitumen system

Operating conditions of this experiment were adapted from the work of Tharanivasan et al. [17]. Therefore, a reasonable set of

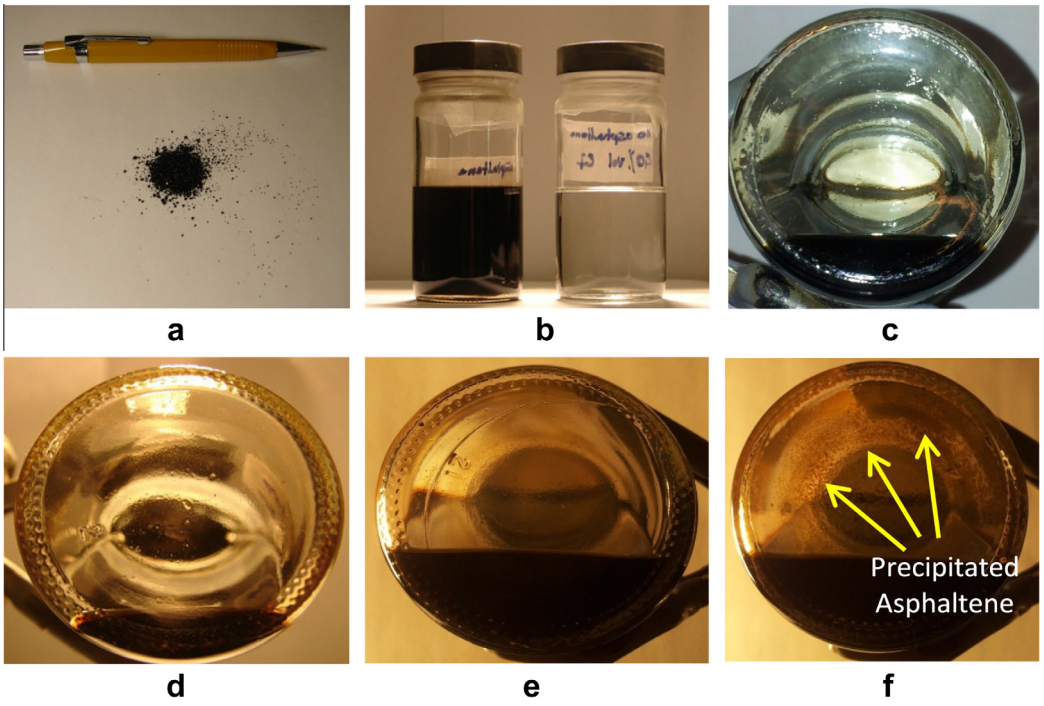

Fig. 5a. Asphaltene solid particles used in preparation of mixtures. **5b.** Sample of 40 vol.% C7, no asphaltene precipitated at the bottom of the jar. **5c.** Sample of 35 vol.% C7, no asphaltene precipitated at the bottom of the jar. **5d.** Sample of 40 vol.% C7, no asphaltene precipitated at the bottom of the jar. **5e.** Sample of 42.5 vol.% C7, few particles of asphaltene observed at the bottom of the jar. **5f.** Sample of 45 vol.% C7, Asphaltene is precipitated at the bottom of the jar.

initial guesses were available for all three unknowns. Using our proposed inverse technique, the calculated pressure matches the experimental pressure quite well. The measured pressure is plotted versus the calculated pressure in Fig. 6. The estimated parameters from our evaluations for this experiment are listed in Table 3.

There are five sets of estimated parameters reported in this table. The first numeric column on the left belongs to the values determined from our semi-analytical model and proposed inverse technique. In the second column, Civan and Rasmussen's [12] long-time approximation solution was applied to determine the values of unknown parameters in our experiment. The third column presents the unknown parameters determined from our technique but for Tharanivasan et al.'s [17] experiment and the fourth column reports the parameters reported in Tharanivasan et al. [17]. Based on Tharanivasan et al.'s work [17] which used

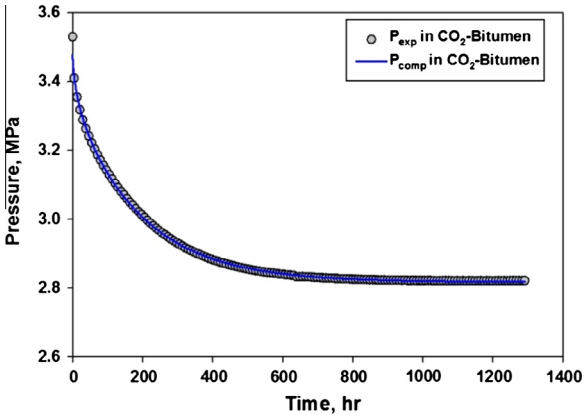

Fig. 6. Experimental pressure decay vs. calculated pressure from the model, case of CO_2–bitumen.

almost the same bitumen, CO_2 solubility versus saturation pressure is linear in the pressure range of our experiment (3.53 MPa and less) and therefore, Henry's law is valid to be applied. The last column presents the diffusion coefficient determined from Upreti and Mehrotra's [18] diffusion experiment at 25 °C and their numerical model.

The diffusion coefficients determined for our experiments are slightly lower than those of Tharanivasan et al.'s. The reasons for this could be minor differences in the bitumen properties and the higher initial pressure of their experiment. They started their pressure decay experiment with a pressure of 4.180 MPa. The determined Henry's constant values for both experiments show a good agreement. Our diffusion coefficient is close to that obtained by Civan and Rasmussen [13]'s evaluation method. However, the interface resistance from our model and experiments is an order of magnitude larger than that of Civan and Rasmussen [12]'s evaluation method and our parameter estimation on Tharanivasan et al. [17]'s experiments. Nonetheless, it shows a good match with the range proposed by Tharanivasan et al. [17] for the mass transfer coefficient in their own experiment. Finally, our determined diffusion coefficient is almost the same as the diffusion coefficient estimated by Upreti and Mehrotra [18].

The calculated sensitivity coefficients are determined and displayed in Fig. 7. This graph reveals useful information about the quality of our parameter estimation. The sensitivity of calculated pressure from our model is determined through Eqs. (16) and (17) for each unknown parameter. One step further is taken here and the sensitivity coefficients are normalized through multiplying the derivative values at each time to their corresponding estimated parameter (Appendix A). These sensitivity coefficients are called normalized/relative sensitivity coefficients [28]. Using this technique, they are shown concisely in one graph and it can be evaluated how sensitive our pressure change is to each of the unknown parameters.

Table 3
Estimated parameters for CO_2–bitumen experiment and their comparison with other works.

Parameters and errors	This experiment our model	This experiment Civan and Rasmussen [12]	Tharanivasan et al. exp. [17] our model	Tharanivasan et al. exp. and estimated values [17]	Upreti and Mehrotra exp. and estimated values [18]
Diffusivity (D), m^2/s	1.339×10^{-10}	1.29×10^{-10}	3.356×10^{-10}	5.7×10^{-10}	1.4×10^{-10}
Mass transfer coef. (k), m/s	2.546×10^{-7}	2.9×10^{-6}	4.369×10^{-6}	$>3.56 \times 10^{-7}$	–
Henry's constant (H), MPa/(kg/m^3)	0.0784	$C_g^* = 37.4$ kg/m^3	0.0787	–	–
Root mean square error	0.0122	–	0.0125	–	–

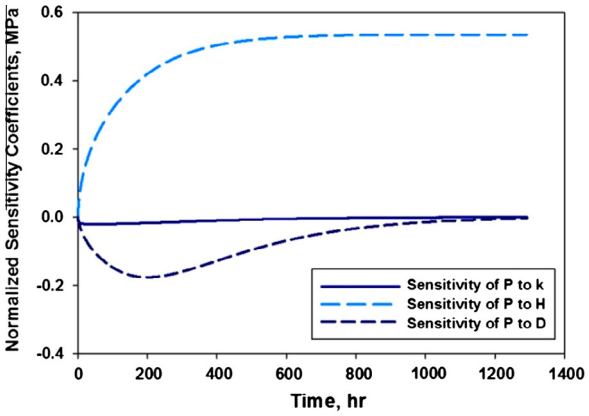

Fig. 7. Normalized/relative sensitivity of the calculated pressure to each of three unknown parameters, case of CO_2/bitumen.

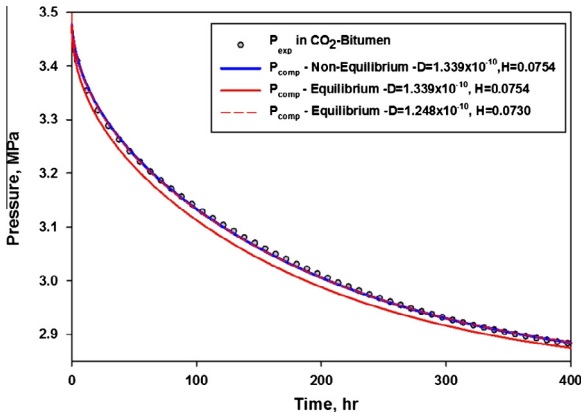

Fig. 8. Comparison of equilibrium and non-equilibrium solutions.

Based on what was stated, the unit of normalized/relative sensitivity coefficients is pressure unit. The first information that is obtained from Fig. 7 is that the relative sensitivity coefficients J_{r1}, J_{r2} and J_{r3} are linearly independent with respect to parameters L_1, L_2 and L_3 (which are k, H and D in this work); i.e., sensitivity of the calculated pressure is investigated with respect to three linearly independent parameters. Determination of Henry's constant and the diffusion coefficient is not difficult through the Levenberg–Marquardt algorithm because the magnitudes of relative sensitivity coefficients are large. It implies that changes of these two parameters affect the estimated pressure significantly. Unlike these two, the magnitude of change of sensitivity coefficients is not significant in the case of the mass transfer coefficient, k. As it is seen in Fig. 7, the solid plot shows that the sensitivity of pressure to k is very small but still not zero. Since it is deviated from zero, the interface resistance has affected the declining pressure. However, its small magnitude change means that finding this parameter through our evaluation is not easy and requires good initial guess to find the correct values of k. The sensitivity to H tends to a finite value after the steady state is reached while it tends zero for the other two parameters. It is because no information is obtained from this measurement for estimation of D and k after their sensitivity curves reach zero. However, sensitivity of pressure to H reaches a finite number as it is only Henry's law that is governing the system after equilibrium.

Dimensionless analysis provides further insight into the information presented in Fig. 7. From the dimensionless analysis for a diffusion process with constant concentration at the interface, once $t_D = Dt/h^2 \cong 1$, the concentration at the bottom of the cell has reached 90% of saturation concentration [39]. Although the concentration is not constant in our case, the same analysis is applied here just to examine our results. Using $t_D = 1$ and the D value from Table 3, the time at which our diffusion process is close to its 90% completion is determined to be around 538 h. From Fig. 7, this time coincides with time when the relative sensitivity coefficient with respect to H reaches almost a constant value. The whole bitumen is expected to be near the saturation condition beyond this time.

If this method is compared with the so-called "slope-intercept" or graphical methods, the main difference is that there should be a priori knowledge of good guesses in cases of small sensitivity coefficients. However, there are two advantages in using this method: (i) it is known how each of the parameters is influencing the pressure decay and (ii) it reveals if the determined resistance value implies a physical resistance or not. This latter is determined through evaluation of sensitivity coefficients again. To explain better, three different pressures decay plots are depicted against the experimental pressure in Fig. 8. The blue[1] solid graph is the calculated pressure with the best estimated parameters in Table 3. Fig. 7 confirms that although small, our calculated pressure is sensitive to k and therefore, it is expected to have resistance at the interface. In this case, a non-equilibrium boundary condition exists at the interface which refers to the presence of a discontinuity between the concentration right above and right below the interface [21]. This leads to a hindrance against diffusion and delays the diffusion process. The root mean square error for this match is 0.01222. Using our proposed mathematical model, if a very large value is given to k, it should work as the equilibrium solution (like Sheikha et al.'s [5]). The red[1] solid line shows the equilibrium case (k goes to ∞) using the same estimated diffusion coefficient and Henry's constant. It is evident that this curve does not match the experimental values as good as the previous match and its root mean square error is 0.01317. This means that our estimated k from the solid blue line is representing presence of interfacial resistance. The red dashed line is matching the experimental pressure (and our non-equilibrium solution too) using the equilibrium solution of Sheikha et al. [5]. As it is seen in Fig. 8, the values determined for the diffusion coefficient and Henry's

[1] For interpretation of color in Figs. 8, 5e, 17, 18 and 20, the reader is referred to the web version of this article.

constant are different than our non-equilibrium solution. The root mean square error in this case is 0.01223. The errors are very similar but which case is correct is the main question. This has been the case in the interpretations of Tharanivasan et al. [16,17] who have compared use of different boundary conditions at the interface. They have no more information to judge and comment on the right boundary condition. However, in this work, based on information from relative sensitivity coefficients, Fig. 7, as the measured pressure shows sensitivity to k, it could be concluded that the interface shows resistance against molecular diffusion and the non-equilibrium case is closer to reality.

The final evaluation on the CO_2–bitumen experiment belongs to verifying the uniqueness of our estimated parameters. Using the three-parameter global search method explained earlier, the accuracy and uniqueness of our determined values for our tests were confirmed. Wide ranges of k, D and H are plotted through two surface plots of our objective function (Eq. (21)) in Figs. 9a and 9b.

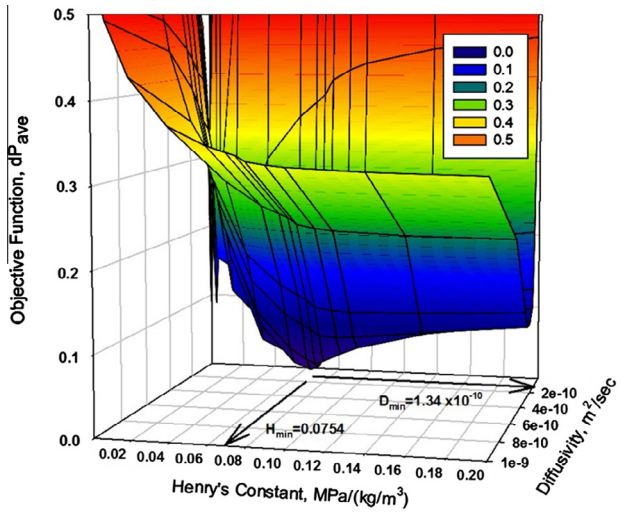

Fig. 9a. Surface plot of objective function in H–D domain ($K_{min} = 0.254 \times 10^{-6}$ m/s) – CO_2/bitumen case.

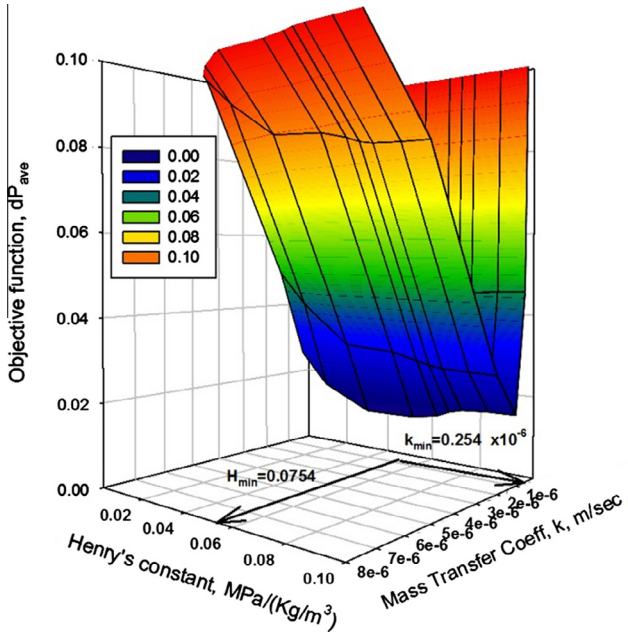

Fig. 9b. Surface plot of objective function in H–K domain ($D_{min} = 1.34 \times 10^{-10}$ m^2/s) – CO_2/bitumen case.

What is important in these two figures is the range of the error plotted in the z-axis for the objective function. The global minimum in Fig. 9a in which D and H are changing is easily obtainable. However, the error range becomes about one-tenth in magnitude in the case of H–K surface. This confirms the challenge of locating the objective function global minimum in presence of the parameter (k), when its change is only marginally affecting our objective function. It should be understood that the uniqueness of estimated parameters needs to be confirmed in applications of such techniques.

4.2. CH_4 in bitumen system

A good initial value was available for the diffusion coefficient of this experiment from Upreti and Mehrotra's [18] work. Fig. 10 depicts how well the calculated pressure matches the experimental results. Fig. 11 displays the sensitivity coefficients against each of three unknown parameters. As it is evident, the pressure sensitivity to k curve stays on zero all the time which means no sensitivity exists with respect to mass transfer coefficients. This implies that the value of pressure is independent from change of k. It can be inferred that equilibrium prevails at the interface and the concentrations above and below the interface reach the same value, instantaneously.

The minimum of the objective function with respect to k is such that for small values of k, it goes down toward a minimum value but once it reaches close to the minimum, it becomes flat. In this

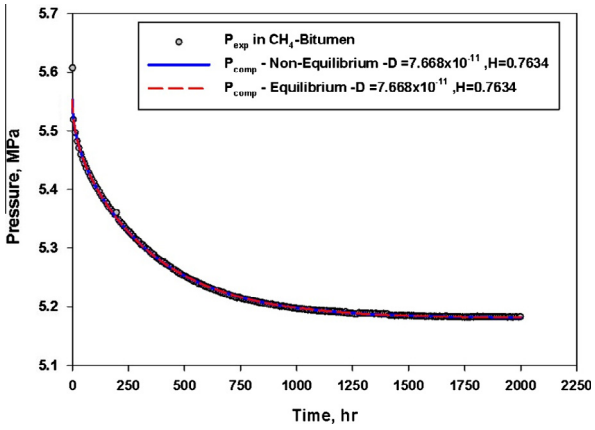

Fig. 10. Experimental pressure decay vs. calculated pressure from the model and comparison of equilibrium and non-equilibrium solutions – case of CH_4/bitumen.

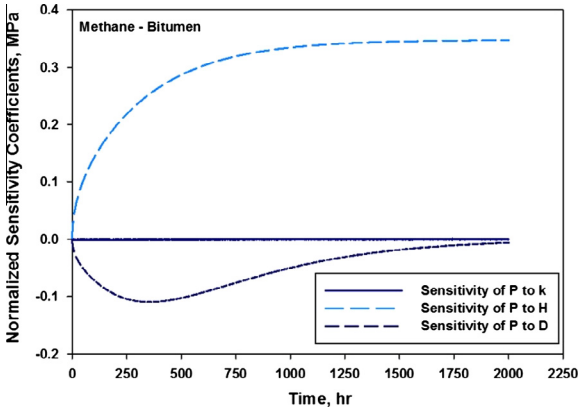

Fig. 11. Normalized/relative sensitivity of the calculated pressure to each of three unknown parameters, case of CH_4/bitumen.

Table 4
Estimated parameters for CH_4–bitumen experiment and their comparison with other works.

Parameters and errors	This experiment our model	This experiment Civan and Rasmussen[12]	Upreti et al. Exp. and estimated values [10] at 25 °C	Henry's constant direct measurement
Diffusivity (D), m^2/s	7.667×10^{-11}	5.23×10^{-11}	8×10^{-11}	–
Mass transfer coef. (k), m/s	Infinity	1.3×10^{-7}	–	–
Henry's constant (H), MPa/(kg/m^3)	0.763	$C_g^* = 6.785$ kg/m^3	–	0.792
Root mean square error	0.000947	–	–	–

region the sensitivity coefficient of pressure with respect to k is very close to zero and therefore, the derivative methods will not be very helpful in finding the direction toward the minimum. In this flat minimum region of the objective function, any initial guess in our minimization algorithm will lead into the same mean square errors. Values of unknown parameters from our method are illustrated in Table 4.

In Table 4, the estimated parameters for Fig. 10's match are reported in the first numerical column on the left. The mass transfer coefficient is reported as infinity. It means that once matched, it does not matter what large number k gets as there is no interfacial resistance. The second column on the left side belongs to the estimation of k and D using Civan and Rasmussen's method. These two values are determined for the given saturation concentration from our experiment. The diffusion coefficients are agreeing with each other while their method produces a value for the mass transfer coefficient. If this reported mass transfer coefficient exists physically, it is in contradiction with the sensitivity analysis of Fig. 11. The third column belongs to Upreti and Mehrotra's reported value for diffusion of methane in Athabasca bitumen. They are reporting a concentration dependent diffusion curve while its average value is very close to what we determined from our experiment and model. Using a recombining cell and PVT measurement equipment, the saturation concentrations at different equilibrium pressures were measured for the same bitumen sample and methane. Fig. 12 displays the results of this study. Henry's law constant determined from this method is 0.792 (reported in the last column on the right) which is close to what we estimated from our model. In view of the data scatter shown in Fig. 12, it is believed that Henry's constant from our mathematical model is more accurate.

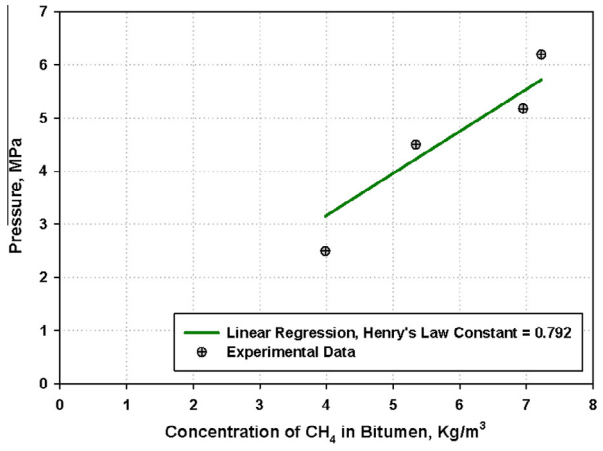

Fig. 12. Estimation of Henry's Law constant through solubility and saturation pressure measurement.

Fig. 10 also compares the fits of the equilibrium model and the non-equilibrium model with the experimental data. Unlike the CO_2–bitumen case, our non-equilibrium solution with any large values for k, would exactly match the equilibrium case while Henry's constant and the diffusion coefficient values are identical. This allows us to conclude that no interfacial resistance exists at the interface of bitumen and methane.

Applying the estimated diffusion coefficient in dimensionless analysis reveals that the time needed to achieve 90% of saturation concentration at the bottom of the cell is around 1,356 h. From Fig. 11, this is the time when the relative sensitivity coefficient with respect to H becomes nearly constant.

4.3. Methane in heptane–toluene–asphaltene system

The main purpose in this section is to explore how the interface resistance affects our pressure measurements and the sensitivity coefficients, and basically, how incipient asphaltene precipitation could affect interface resistance which is detectable through this technique. Using our inverse technique for all seven experiments (Table 2), the values of unknown parameters were measured and are reported in Table 5. The initial guesses for Henry's constant were determined from a simple calculation on the amount of dissolved gas at equilibrium pressure. For the sake of brevity, only the pressure result of experiment 6 is plotted in Fig. 13. The quality of pressure matching is evaluated through the root mean square error in Table 5. Fig. 14 displays the sensitivity of calculated pressure to the three unknowns. Like the previous cases, the pressure is quite sensitive to the changes in the diffusion coefficient and Henry's constant. Its sensitivity to the mass transfer coefficient, k, although small, is still significant.

In Fig. 14, the relative sensitivity of pressure to D goes asymptotically to zero around the 40th hour. This means that basically no more information can be obtained from measurements taken for time beyond 40th hours for estimation of D. This is also true for estimation of k, which is illustrated more evidently in Fig. 15. It is desirable to have linearly-independent sensitivity coefficients with large magnitude, so that the inverse problem is not very sensitive to measurement errors and accurate estimation of parameters is determined. Fig. 15 illustrates the magnitude of the relative sensitivity coefficients of pressure with respect to k, as

Table 5
Estimated parameters for all experiments in diffusion of methane in C7–toluene–asphaltene mixture.

Parameters and errors	30 vol.% C7	32.5 vol.% C7	35 vol.% C7	37.5 vol.% C7	40 vol.% C7	42.5 vol.% C7	45 vol.% C7
D, $m^2/s \times 10^9$	5.954	6.195	6.281	6.674	6.885	6.720	6.560
k, $m/s \times 10^5$	9.15	8.41	2.95	1.27	1.04	3.50	4.85
H, MPa/(kg/m^3)	0.313	0.308	0.310	0.319	0.313	0.298	0.295
RMS error $\times 10^3$	1.96	0.95	1.17	1.36	1.22	1.21	1.61

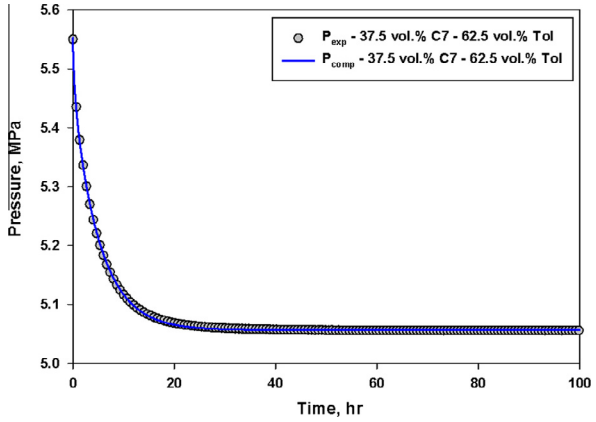

Fig. 13. Experimental pressure decay vs. calculated pressure from the model, case of 37.5 vol.% C7 – 62.5 vol.% toluene.

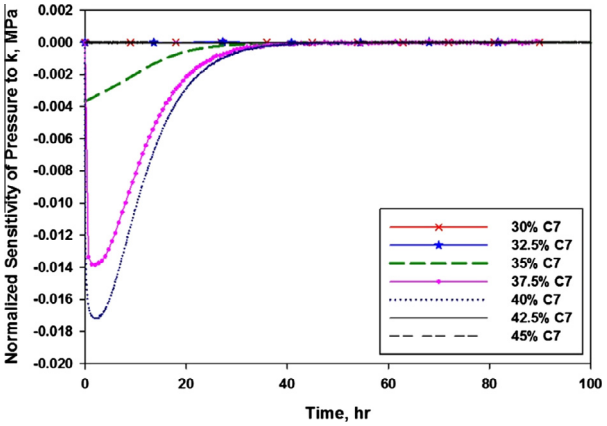

Fig. 15. Normalized/relative sensitivity of the calculated pressure to *k*, all cases.

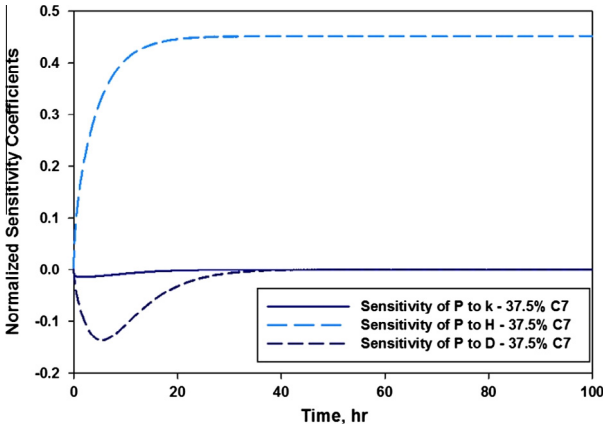

Fig. 14. Normalized/relative sensitivity of the calculated pressure to each of three unknown parameters, case of 37.5 vol.% heptane – 62.5 vol.% toluene.

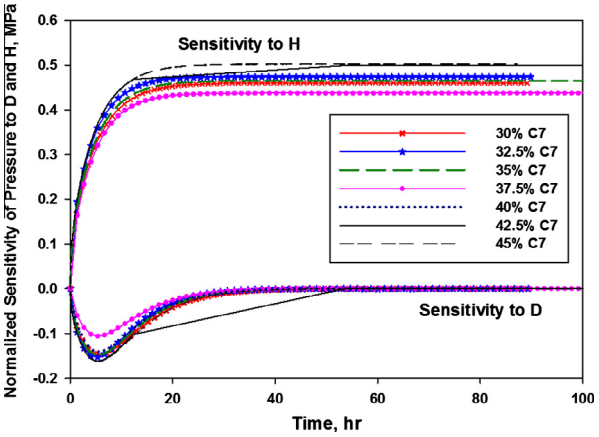

Fig. 16. Normalized/relative sensitivity of the calculated pressure to *D* and *H*, all cases.

explained, for all seven cases. The top three magnitudes belong to the cases of 40 vol.% C7, 37.5 vol.% C7 and 35 vol.% C7, respectively. As it is seen in this figure, pressures in these three cases 35, 37.5 and 40 vol.% C7 show sensitivity to the changes of *k*, while the other cases 32, 32.5, 42.5 and 45 vol.% C7, show almost zero sensitivity. Our proposed inverse solution was able to only obtain values of mass transfer coefficients for the cases of 35, 37.5 and 40 vol.% C7 easily, even when the initial conditions were not close to the optimum parameters. However, for the other four cases, we were able to use this method only if a close initial guess value for *k* was used. Otherwise, our proposed algorithm was not able to converge to a unique minimum number. This was because the calculated pressure was not very sensitive to *k* values in this region. Our proposed search method was utilized to find the definite values of *k* for these four experiments to examine if the estimated values from the Levenberg–Marquardt algorithm are correct and unique. The range of search for *k* is from 10^{-8} to 10^{-1} m/s. Results of these evaluations and the estimated parameters are shown in Table 5 and Figs. 15 and 16.

Fig. 17 displays the relative sensitivity coefficients of pressure change to *D* and *H*. Unlike, the case of sensitivity to *k*, it is evident that the sensitivity coefficient plots are almost the same and large in magnitude (in comparison with values in Fig. 15) in all cases. That is why the Levenberg–Marquardt algorithm could easily locate the optimum parameters for diffusivity and Henry's constant value.

Values presented in Table 5 are plotted through bar charts in Figs. 17, 18 and 20. The qualities of pressure matching were quite acceptable for all seven cases. Fig. 17 shows that the diffusion coefficient becomes large once it gets close to 40% vol. C7 and then decreases. The ranges of changes in diffusion coefficient are very small. In order to distinguish if these changes are due to error of estimation or not, the error bars were determined for two sensitive simplifying assumptions which have been used in our mathematical model namely; "no volume change in liquid" and "constant gas compressibility coefficients" [21]. Using our cathetometer, the height of the liquid mixture at the beginning and end of each experiment was recorded. Peng–Robinson equation of state was used to include changes of *Z* with pressure in the range of our pressure decline. The values of liquid mixture height and gas compressibility which the unknown parameters are estimated for to show the errors of the above simplifying assumptions are presented in Table 6. The error bars plotted in Figs. 17, 18 and 20 are displaying these changes. In each figure, the blue bars (the left column in each pair) are showing the error bars due to the volume change in the liquid mixture (swelling) and the green bars (the right column in each pair) are displaying the error bars in *Z* alteration due to pressure change. As it is evident, the errors due to the change of *Z* are insignificant in comparison with the errors for height changes in the cases of *H* and *D* estimations. In Fig. 17, the errors are in the same ranges.

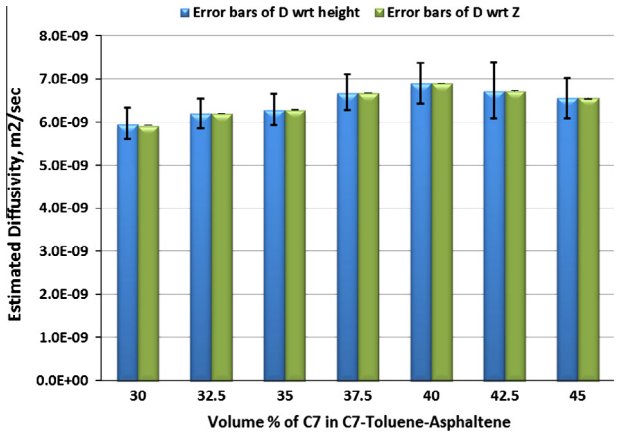

Fig. 17. Error bars for the changes of estimated diffusion coefficients with uncertainties in height and gas compressibility factor (Z).

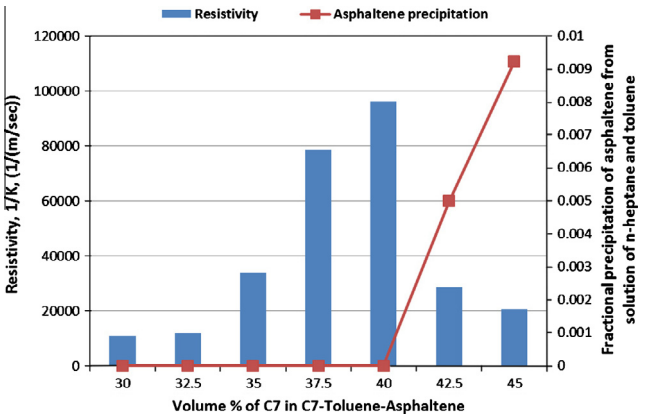

Fig. 19. Interface resistance ($1/k$) determined from our model vs. fractions of asphaltene precipitated by Alboudwarej et al. [38].

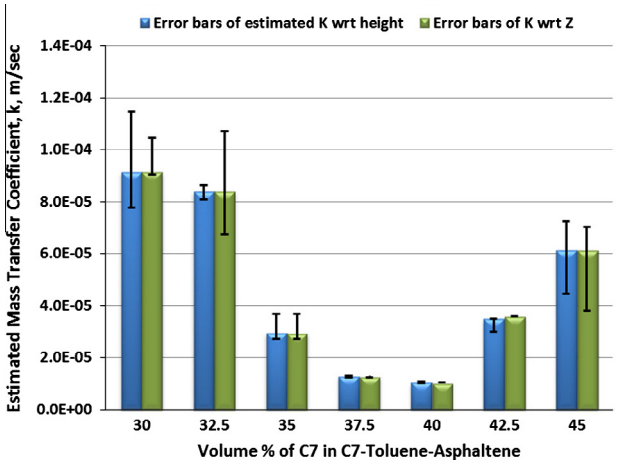

Fig. 18. Error bars for the changes of mass transfer coefficients with uncertainties in height and gas compressibility factor (Z).

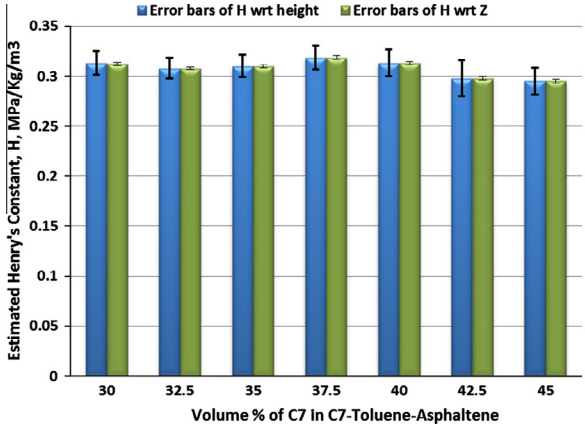

Fig. 20. Error bars for the changes of Henry's law constant with uncertainties in height and Z (gas compressibility).

Including the errors, Fig. 17 shows that diffusion coefficients of methane in the mixture are essentially the same within the error bars, even though this figure gives the impression of increasing diffusivity toward the 40% C7 case. A small increase could be due to change in the amount of toluene. Fig. 18 is giving most of the information that are sought. As it is seen, the interface resistance becomes larger (k becomes smaller) as the concentration gets closer to the onset of de-asphalting. The minimum value of k belongs to 40 vol.% C7. Based on our observations from 1.5 days after the sample preparation, the case with the highest C7 concentration that had no precipitated asphaltene particle was this 40 vol.% C7 case. This is in agreement with what was discussed about surface active molecules and adsorption phenomena. Once the liquid concentration becomes closer to the onset of asphaltene precipitation, more surface active asphaltene molecules are adsorbed to the interface. This could result in higher resistance in these conditions. Therefore, the k value declining trend from 30 to 40 vol.% C7 confirms our hypothesis. Beyond 40 vol.% C7, asphaltene precipitation was observed in the preparation phase of samples containing 42.5 and 45 vol.% C7. The mass transfer coefficient value starts to rise again which means less interface resistance. This could be because once the asphaltene starts to precipitate, both the bulk solution concentration and the interface concentration decrease. This explains why the interface resistance becomes smaller again.

Table 6
Liquid mixture swelling data and changes in gas compressibility factor in certain gas dissolution amounts.

	Diffusion of methane in C7–toluene–asphaltene mixture	Cases mixture h–z factor	30 vol.% C7	32.5 vol.% C7	35 vol.% C7	37.5 vol.% C7	40 vol.% C7	42.5 vol.% C7	45 vol.% C7
1	Liquid height (mm)	Final height at C_g^*	18.41	18.06	18.47	18.36	18.78	19.62	19.27
		Average height[a]	17.87	17.57	17.92	17.81	18.15	18.72	18.61
		Initial height	17.34	17.09	17.38	17.26	17.52	17.82	17.95
		Height increment	1.07	0.97	1.09	1.10	1.26	1.80	1.32
2	Gas compressibility, z	z of initial P	0.885	0.885	0.884	0.883	0.884	0.883	0.885
		Average z[a]	0.888	0.889	0.888	0.888	0.888	0.888	0.889
		z of equilibrium P	0.893	0.893	0.892	0.892	0.892	0.894	0.894

[a] Data used in the estimation of unknown parameters presented by bar charts in Figs. 17, 18 and 20.

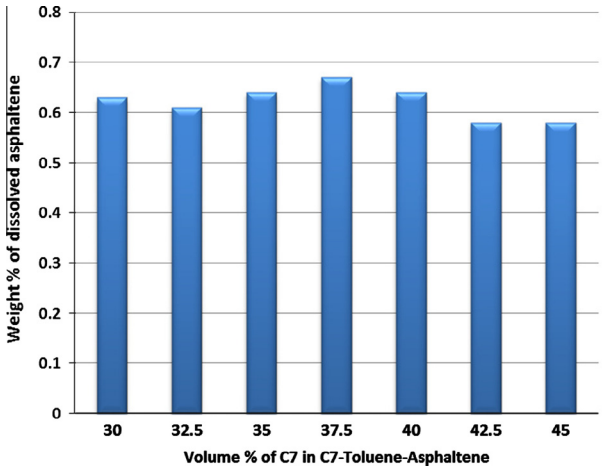

Fig. 21. Weight % of asphaltene added/dissolved into C7–toluene mixture in each case.

The inverse values of the estimated mass transfer coefficients are plotted along with the amounts of precipitated asphaltenes (from Alboudwarej et al. [38]) in Fig. 19. This graph shows that our speculation about the incipient de-asphalting phenomena as one of the reasons for presence of resistance at the interface is valid.

Henry's law constant values which represent the amounts of dissolution of methane in the mixture are plotted in Fig. 20. The changes seem to be very random and are mostly within the error bars. However, based on our observations, an apparent relation was found between these values and the amount of asphaltene added/dissolved in each sample during preparation phase. Based on Fig. 5 asphaltene was fully dissolved in all cases except 42.5 and 45 vol.% C7, where precipitation was observed during samples' preparation. If the weight % of solid asphaltene added to each sample is plotted for each case, Fig. 21 is obtained. A correlation is observed between the value alterations in Figs. 20 and 21. What is inferred from these two is that solubility is higher (H is smaller) in cases where less asphaltene is added to the mixture. This sounds reasonable, because when more asphaltene is dissolved in the mixture, less capacity remains for the molecules of gas.

5. Concluding remarks

An improved analytical solution is applied for the pressure decay experiment which models both equilibrium (no interfacial resistance) and non-equilibrium boundary conditions. This model accounts for the relationship between gas cap pressure decline and concentration at the interface. An additional advantage is that we directly deal with pressure values and there is no need for extra calculations of the mass of gas dissolved in oil to predict the unknown mass transfer parameters.

Results of this model lead to improved interpretations of pressure decay tests and reliable estimation of the diffusion parameters. Through the proposed inverse technique, three mass transfer parameters could be measured through running one experiment. Sensitivity coefficient analysis is a very powerful tool to disclose information about (i) the level of sensitivity of our predicted pressure with respect to each of the unknown mass transfer parameters (ii) ease/feasibility of calculating each of the unknown parameters through pressure decay measurement (iii) the period of experimental data that gives us information for estimation of unknown parameters and, therefore, the required period over which the experiment should be conducted, and (iv) whether or not the differences in calculated values could be in the range of experimental errors and need to be further investigated.

Interface resistance may exist in problems of solvent diffusion into the bitumen like the case of CO_2 in bitumen. Hindrance in gas diffusion may also be reported numerically while it does not exist physically like the case of CH_4 in bitumen. Nevertheless, it helps finding a more accurate diffusion coefficient. Measurements of mass transfer parameters in the heptane–toluene–asphaltene mixtures showed that closer to onset of asphaltene precipitation, the interface resistance becomes larger. This could hinder the solvent diffusion processes in bitumen.

Acknowledgements

The first author would like to thank Mr. Jordan D. Woloschuk and Mr. Ilia Chaikine for their assistance in lab works. Useful comments and support of Dr. Harvey Yarranton is highly appreciated. Asphaltene particle was provided by Asphaltene and Emulsion Research Lab. The financial support by National Sciences and Engineering Research Council (NSERC) and NSERC/AIEES/Foundation CMG/AITF(iCORE) chairs is acknowledged.

Appendix A. Jacobian matrix and normalized/relative sensitivity coefficients

Jacobian or sensitivity matrix plays a very important role in parameter estimation problems. For our problem, the components of sensitivity matrix are defined as Eq. (A.1).

$$J\left(\vec{L}\right) = \left[-\frac{\partial \vec{P_{\text{comp}}}^{T}\left(\vec{L}\right)}{\partial \vec{L}}\right]^{T} = \begin{bmatrix} \frac{\partial P_{\text{comp1}}}{\partial L_1} & \frac{\partial P_{\text{comp1}}}{\partial L_2} & \frac{\partial P_{\text{comp1}}}{\partial L_3} \\ \frac{\partial P_{\text{comp2}}}{\partial L_1} & \frac{\partial P_{\text{comp2}}}{\partial L_2} & \frac{\partial P_{\text{comp2}}}{\partial L_3} \\ \frac{\partial P_{\text{comp3}}}{\partial L_1} & \cdots & \vdots \\ \cdots & \cdots & \vdots \\ \frac{\partial P_{\text{compn}}}{\partial L_1} & \frac{\partial P_{\text{compn}}}{\partial L_2} & \frac{\partial P_{\text{compn}}}{\partial L_3} \end{bmatrix}_{n\times 3} \tag{A.1}$$

The sensitivity coefficient J_{ij} can be any of the elements of the Jacobian matrix and is a measure of sensitivity of the computed pressure P_{compi} with respect to changes in the parameter L_j. A small value of the magnitude of J_{ij} indicates that large changes in the value of the diffusion coefficient, Henry's law constnat and mass transfer coefficient yield small changes in P_{compi}. Based on this, estimation of any of these parameters is extremely difficult in such a case, because basically the same pressure value is obtained for a wide range of any of parameter values. When the sensitivity coefficients are small, $|J^T J| \approx 0$, the inverse problem is called ill-conditioned [28]. The most desirable coefficients are linearly-independent sensitivity coefficients with large magnitudes, such that the inverse problem is not very sensitive to measurement errors.

The value of sensitivity coefficients as components of the Jacobian matrix was approximated through finite difference methods using central differences as follows:

$$J_{i1} = \frac{P_{comp}(t_i, L_1 + \varepsilon L_1, L_2, L_3) - P_{comp}(t_i, L_1 - \varepsilon L_1, L_2, L_3)}{2\varepsilon L_1} \tag{A.2.1}$$

$$J_{i2} = \frac{P_{comp}(t_i, L_1, L_2 + \varepsilon L_2, L_3) - P_{comp}(t_i, L_1, L_2 - \varepsilon L_2, L_3)}{2\varepsilon L_2} \tag{A.2.2}$$

$$J_{i3} = \frac{P_{comp}(t_i, L_1, L_2, L_3 + \varepsilon L_3) - P_{comp}(t_i, L_1, L_2, L_3 - \varepsilon L_3)}{2\varepsilon L_3} \tag{A.2.3}$$

In this problem, three parameters are involved with different orders of magnitude. This creates difficulties in their comparison and identification of linear dependence [28]. Use of dimensionless relative sensitivity coefficients is one way to alleviate this difficulty.

$$\overrightarrow{J}_{r_j} = L_j \frac{\partial \overrightarrow{P}}{\partial L_j} \tag{A.3}$$

In this case, the relative sensitivity coefficients have the unit of pressure, MPa. Therefore, they are compared as having the magnitude of the measured pressure as a basis and could be plotted versus time like in Figs. 7, 11 and 14 to be compared. Note that the elements of relative sensitivity vectors (for each j) are not used in the Jacobian matrix and are only used to compare the linear dependence of the parameters and the level of sensitivity of measured pressure to each of the parameters.

References

[1] Etminan SR, Maini BB, Chen Z, Hassanzadeh H. Constant-pressure technique for gas diffusivity and solubility measurements in heavy oil and bitumen. Energy Fuels 2010;24(1):533–49.
[2] Schmidt T. Mass transfer by diffusion. AOSTRA Technical Handbook on Oil Sands. Bitumens and Heavy Oils; 1989.
[3] Song L, Kantzas A, Bryan J. Experimental measurement of diffusion coefficient of CO_2 in heavy oil using X-ray computed-assisted tomography under reservoir conditions; 2010.
[4] Song L, Kantzas A, Bryan J. Investigation of CO_2 diffusivity in heavy oil using X-ray computer-assisted tomography under reservoir conditions; 2010.
[5] Sheikha H, Pooladi-Darvish M, Mehrotra AK. Development of graphical methods for estimating the diffusivity coefficient of gases in bitumen from pressure-decay data. Energy Fuels 2005;19(5):2041–9.
[6] Yang C, Gu Y. New experimental method for measuring gas diffusivity in heavy oil by the dynamic pendant drop volume analysis (DPDVA). Indust Eng Chem Res 2005;44(12):4474–83.
[7] Jamialahmadi M, Emadi M, Muller-Steinhagen H. Diffusion coefficients of methane in liquid hydrocarbons at high pressure and temperature. J Petrol Sci Eng 2006;53(1–2):47–60.
[8] Riazi MR. A new method for experimental measurement of diffusion coefficients in reservoir fluids. J Petrol Sci Eng 1996;14(3–4):235–50.
[9] Sachs W. The diffusional transport of methane in liquid water: method and result of experimental investigation at elevated pressure. J Petrol Sci Eng 1998;21(3–4):153–64.
[10] Upreti SR, Mehrotra AK. Experimental measurement of gas diffusivity in bitumen: results for carbon dioxide. Indust Eng Chem Res 2000;39(4):1080–7.
[11] Yang D, Tontiwachwuthikul P, Gu Y. Dynamic interfacial tension method for measuring gas diffusion coefficient and interface mass transfer coefficient in a liquid. Indust Eng Chem Res 2006;45(14):4999–5008.
[12] Civan F, Rasmussen M. Determination of gas diffusion and interface-mass transfer coefficients for quiescent reservoir liquids. SPE J 2006;11(1):71–9.
[13] Civan F, Rasmussen ML. Accurate measurement of gas diffusivity in oil and brine under reservoir conditions. Pape
r SPE; 2001. p. 67319.
[14] Civan F, Rasmussen ML. Improved measurement of gas diffusivity for miscible gas flooding under nonequilibrium vs. equilibrium conditions. Paper SPE; 2002. p. 75135.
[15] Sheikha H, Mehrotra AK, Pooladi-Darvish M. An inverse solution methodology for estimating the diffusion coefficient of gases in Athabasca bitumen from pressure-decay data. J Petrol Sci Eng 2006;53(3–4):189–202.
[16] Tharanivasan AK, Yang C, Gu Y. Comparison of three different interface mass transfer models used in the experimental measurement of solvent diffusivity in heavy oil. J Petrol Sci Eng 2004;44(3–4):269–82.
[17] Tharanivasan AK, Yang C, Gu Y. Measurements of molecular diffusion coefficients of carbon dioxide, methane, and propane in heavy oil under reservoir conditions. Energy Fuels 2006;20(6):2509–17.
[18] Upreti SR, Mehrotra AK. Diffusivity of CO_2, CH_4, C_2H_6 and N_2 in Athabasca bitumen. Can J Chem Eng 2002;80(1):116–25.
[19] Zhang Y, Hyndman C, Maini B. Measurement of gas diffusivity in heavy oils. J Petrol Sci Eng 2000;25(1–2):37–47.
[20] Haugen KB, Firoozabadi A. Mixing of two binary nonequilibrium phases in one dimension. AIChE J 2009;55(8):1930–6.
[21] Etminan SR, Pooladi-Darvish M, Maini BB, Chen Z. Modeling the interface resistance in low soluble gaseous solvents-bitumen systems. Fuel 2012;105:672–87.
[22] Civan F, Rasmussen ML. Rapid simultaneous evaluation of four parameters of single-component gases in nonvolatile liquids from a single data set. Chem Eng Sci 2009;64(23):5084–92.
[23] Rasmussen ML, Civan F. Parameters of gas dissolution in liquids obtained by isothermal pressure decay. AIChE J 2009;55(1):9–23.
[24] Reamer H, Opfell J, Sage B. Diffusion coefficients in hydrocarbon systems methane–decane–methane in liquid phase-methane–decane–methane in liquid phase. Indust Eng Chem 1956;48(2):275–82.
[25] Stehfest H. Algorithm 368: numerical inversion of Laplace transforms [D5]. Commun ACM 1970;13(1):47–9.
[26] Alifanov OM. Inverse heat transfer problems. Springer-Verlag; 1994.
[27] Loulou T, Adhikari B, Lecomte D. Estimation of concentration-dependent diffusion coefficient in drying process from the space-averaged concentration versus time with experimental data. Chem Eng Sci 2006;61(22):7185–98.
[28] Özisik MN, Orlande HRB. Inverse heat transfer: fundamentals and applications. Taylor & Francis; 2000.
[29] Hoffman JD. Numerical methods for engineers and scientists. Marcel Dekker; 2001.
[30] Mittrapiyanuruk P. A memo on how to use the levenberg-marquardt algorithm for refining camera calibration parameters. Website, <http://www.cobweb.ecn.purdue.edu/~kak/courses-i-teach/ECE661/HW5LMhandout.pdf>; 2006.
[31] Jeribi M et al. Adsorption kinetics of asphaltenes at liquid interfaces. J Colloid Interface Sci 2002;256(2):268–72.
[32] Eley D, Hey M, Lee M. Rheological studies of asphaltene films adsorbed at the oil/water interface. Colloids Surfaces 1987;24(2):173–82.
[33] Borwankar R, Wasan D. The kinetics of adsorption of surface active agents at gas–liquid surfaces. Chem Eng Sci 1983;38(10):1637–49.
[34] Escrochi M, Mehranbod N, Ayatollahi S. The gas–oil interfacial behavior during gas injection into an asphaltenic oil reservoir. J Chem Eng Data 2013;58(9):2513–26.
[35] Buckley J et al. Asphaltene precipitation and solvent properties of crude oils. Petrol Sci Technol 1998;16(3–4):251–85.
[36] Carlos da Silva Ramos A et al. Interfacial and colloidal behavior of asphaltenes obtained from Brazilian crude oils. J Petrol Sci Eng 2001;32(2):201–16.
[37] Bauget F, Langevin D, Lenormand R. Dynamic surface properties of asphaltenes and resins at the oil–air interface. J Colloid Interface Sci 2001;239(2):501–8.
[38] Alboudwarej H et al. Regular solution model for asphaltene precipitation from bitumens and solvents. AIChE J 2003;49(11):2948–56.
[39] Crank J. The mathematics of diffusion, vol. 1. Clarendon press Oxford; 1979.